Fano enhancement of unlocalized nonlinear optical processes

Mehmet Günay,[1,2] Ahmet Cicek,[1] Nurettin Korozlu,[1] Alpan Bek,[3,4] and Mehmet Emre Tasgin[2]
[1]*Department of Nanoscience and Nanotechnology, Faculty of Arts and Science, Burdur Mehmet Akif Ersoy University, 15030 Burdur, Turkey*
[2]*Institute of Nuclear Sciences, Hacettepe University, 06800 Ankara, Turkey*
[3]*Department of Physics, Middle East Technical University, 06800 Ankara, Turkey*
[4]*Center for Solar Energy Research and Applications, Middle East Technical University, 06800 Ankara, Turkey*

(Received 2 May 2020; accepted 22 November 2021; published 7 December 2021)

Field localization boosts nonlinear optical processes at the hot spots of metal nanostructures. Fano resonances can further enhance these "local" processes taking place at the hot spots. However, in conventional nonlinear materials, the frequency conversion takes place along the entire crystal body. That is, the conversion process is "unlocalized." The path interference (Fano resonance) schemes developed for localized processes become useless in such materials. Here, we develop Fano enhancement schemes for unlocalized nonlinear optical processes. We show that three-orders-of-magnitude Fano enhancement *multiplies* the enhancements achieved via field-trapping techniques, e.g., in epsilon-near-zero materials. We demonstrate the phenomenon both analytically and using numerical solutions of Maxwell's equations. The agreement between the two solutions is impressive. We observe that the interference scheme for unlocalized processes is richer than that for the local processes. The method can be employed for any kind of nonlinear optical conversion. Moreover, Fano enhancement can be continuously controlled by an applied voltage.

DOI: 10.1103/PhysRevB.104.235407

I. INTRODUCTION

The past two decades have witnessed fascinating progress in two research areas, namely classical and quantum plasmonics [1]. One phenomenon is common to both research areas: strong field localization at metal nanoparticle (MNP) hot spots. The localized field intensity can be five to seven orders of magnitude stronger than the intensity of the incident light in the nm-sized hot spots [2,3]. The (classical) plasmonics employs field enhancement for ultrahigh sensing [4], hot-spot-sized optical resolution [5,6], high-frequency communication technologies [7], and to achieve extreme nonlinearity enhancements [8]. Nonlinear optical processes taking place at the hot spots can be enhanced with the second power of the local intensity, because both the input and the converted fields are localized [9–11]. This makes plasmonics an attractive field for nonlinear optics.

Quantum plasmonics utilizes strong field localization for enhanced light-matter interaction. When a quantum emitter (QE)—e.g., a molecule, a quantum dot (QD), or a color-center—is placed at the hot spot, it creates path interference effects called Fano resonances [12–16]. Fano resonances can provide control over both the linear [17] and the nonlinear [18–23] response of metal nanostructures. The nonlinearity enhancement provided by the local field enhancement (in classical plasmonics) can also be multiplied by a Fano-enhancement factor that can be three orders of magnitude depending on the choice of the QE level spacing.

The Fano resonances studied so far control the "local" nonlinear processes that take place at the hot spots. However, conventional frequency converters are nonlinear crystals where conversion takes place along the entire crystal body. The path interference (Fano) enhancement schemes for localized nonlinear processes become useless for such nonlinear crystals. In this work, we demonstrate theoretically and computationally how Fano control of such "unlocalized" nonlinear processes can be made possible.

Nonlinear processes taking place in conventional frequency converters can also be enhanced by concentrating the field into the crystals. Embedding plasmonic nanoparticles (NPs) into nonlinear crystals can enhance the conversion [24,25] by localizing the field near the NPs. A better method employs epsilon-near-zero (ENZ) materials. An ENZ medium not only greatly enhances the field inside the frequency converter [26–29], but it also relieves the phase-matching condition [30] in longer nonlinear crystals. Moreover, recently explored longitudinal ENZ (LENZ) materials can provide stronger second-harmonic (SH) and third-harmonic (TH) conversion enhancements via circumventing material losses [31]. In these (more convenient) materials, the enhanced field is confined in the body of the material rather than being localized at nm-sized hot spots. One can also combine the two field-trapping methods [32] for stronger enhancement rates. These methods rely on the enhancement of the field inside the nonlinear crystal. The presence of an unlocalized Fano-enhancement method, compatible with such materials and multiplying all other enhancement factors, would be very beneficial in achieving high conversion factors in nonlinear crystals.

In this paper, we develop such a Fano-control mechanism for the *further* enhancement of "unlocalized" nonlinear optical processes taking place in conventional frequency

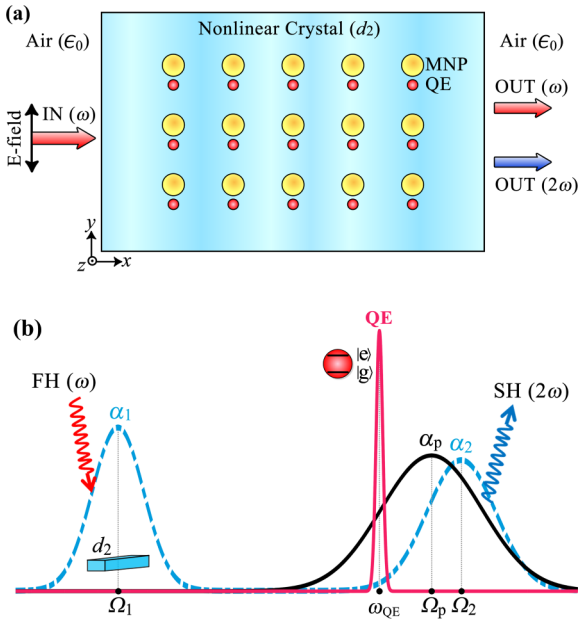

FIG. 1. Fano enhancement scheme for a second-harmonic converting crystal. (a) MNP-QE dimers are embedded in a nonlinear crystal with a second-order susceptibility d_2. The dimers interact with the converted (2ω) field and introduce path interference (Fano) effects. The crystal is pumped with a y-polarized laser of frequency ω. The nonlinear process can be enhanced without exploiting field-trapping techniques. (b) The diagram for the crystal ($\alpha_{1,2}$) and the plasmon (α_p) modes of resonances $\Omega_{1,2}$ and Ω_p, and the QE resonance ω_{QE}. The converted field interacts with the MNP (α_p), and the MNP couples with the QE.

converters [33]. We show that MNP-QE dimers can introduce path interference (Fano) effects in unlocalized nonlinear processes. With the appropriate choice of the QE's level spacing ω_{QE}, nonlinear process can be enhanced, e.g., by three orders of magnitude. This enhancement takes place *without* increasing the fundamental (first-harmonic) field intensity in the crystal. In other words, our method further enhances ($\sim$1000$\times$) the nonlinear field, which is already enhanced via field-trapping techniques, e.g., in MNP-doped [24,25] and ENZ/LENZ materials [26,27,29,31]. More explicitly, for instance, 10^4 times conversion enhancement in an ENZ material [26,27,29,31] can be further multiplied by a factor of $\sim$1000, yielding a total enhancement ratio of 10^7. The method can be applied to both photonic and nanophotonic (smaller) devices.

We consider a system where MNP-QE dimers are embedded in a crystal body; see Fig. 1(a). We utilize the MNPs as strong interaction centers for the "converted" (e.g., SH) field. MNPs collect the *unlocalized* converted field into the hot spots and make it interact with the QE. Intriguingly, we find that MNP-QE dimers can control the produced nonlinear field throughout the entire crystal body.

Our numerical (COMSOL [34]) simulations clearly demonstrate that the SH (2ω) field intensity can be enhanced by a factor of $\sim$1000 *without increasing* the fundamental frequency (FF, ω) field inside the crystal. We not only demonstrate the phenomenon via numerical solutions of Maxwell's equations, but we also explain the physics behind the Fano enhancement mechanism, which multiplies the enhancements created by the field-trapping techniques [24–29,31,32]. We present a simple analytical expression for the converted (SH) field amplitude. We demonstrate that further enhancement occurs due to the cancellations in the denominator of this expression without changing the FF field intensity. The results for the numerical solutions of Maxwell's equations and the analytical model match successfully. The analytical model also shows that the interference scheme for the control of the "unlocalized" nonlinear processes is different from the scheme for the control of localized processes. It provides a richer cancellation scheme.

It is worth noting that we use the term "Fano enhancement" to refer to the further enhancement that multiplies other enhancement factors appearing due to the field-trapping techniques. As explicitly demonstrated in the text, Fano enhancement appears due to the cancellations in the denominator of the nonlinear response, and it is independent of the FF field enhancements. The total enhancement includes both effects.

The exceptional features of our method can be summarized as follows: (i) The path interference (Fano) can further enhance an unlocalized nonlinear process that is already enhanced via field-trapping techniques [24–29,31,32]. (ii) The Fano enhancement scheme does not increase the FF (ω) field intensity. This allows an $\sim$1000 times further enhancement for the crystals already operating in the upper temperature limits. (iii) Since a $\sqrt{1000} \simeq 33$ times smaller pump intensity would suffice for efficient frequency conversion, battery lifetimes of portable lasers would be extended significantly. (iv) Moreover, the Fano enhancement factor can be *continuously tuned* around its peak value via an applied voltage. The applied voltage could tune the QE resonance ω_{QE}, which in turn could be used to switch the Fano enhancement. (v) Above all, the Fano enhancement scheme we demonstrate for the SHG process can be employed also for higher-order nonlinear optical processes. For instance, we demonstrate path interference schemes also for third-harmonic generation and four-wave mixing in Ref. [35].

Here, we work out the path interference effects in the nonlinear response of materials. A linear version of the effect would be associated with the Fano lasers [36,37] if one removes the MNP from the interference scheme. A photonic crystal Fano laser made of a line defect waveguide (active medium) coupled to a narrow linewidth nanocavity is studied in the literature. The nanocavity introduces the Fano effect, which enables an interesting self-pulsing phenomenon [37] and a high-frequency modulation [36]. In such a photonic crystal system, one can also study the nonlinear Fano effect by choosing the nanocavity resonance near the converted frequency. In such a system, however, the nanocavity resonance is not voltage-tunable. Thus, the nanocavity resonance has to be manufactured carefully, and it is hard to arrange the Fano resonance peak.

II. RESULTS

A. Dynamics of the system

In particular, we consider the SHG process from a nonlinear crystal, see Fig. 1(a), in which MNP-QE dimers are

embedded for the Fano enhancement. The dynamics of the system and the interactions can be described as follows.

A laser of frequency ω (fundamental, $\lambda = 1064$ nm) pumps the α_1-mode of the nonlinear crystal. The pump excites the ω frequency photons in the α_1-mode; see Fig. 1(b). The resonance of the α_1 crystal mode is Ω_1. Here, α_1 refers to the amplitude of the fundamental frequency (FF) field inside the crystal. The crystal performs SHG: two ω photons in the crystal (α_1-mode) combine to generate a 2ω photon ($\lambda/2 = 532$ nm) in the α_2-mode of the crystal. The resonance of the α_2 crystal mode is Ω_2. α_2 refers to the amplitude of the SH field inside the crystal. There can exist other modes in the crystal, but we refer merely to the relevant ones: the pumped mode α_1 and the mode α_2 into which SHG takes place.

The resonance frequency of the MNP plasmon mode Ω_p is chosen at about the SH frequency 2ω, so Ω_p is also about the resonance frequency of the α_2 crystal mode Ω_2; see Fig. 1(b). The SH-generated field interacts strongly (of strength g) with the MNP. The MNP localizes the generated SH field into its hot spot as a plasmonic near-field. α_p refers to the amplitude of the plasmon excitation on the MNP. The plasmon mode displays a localized near-field at the MNP hot spot. The QE is placed at this hot spot. Thus, the QE interacts strongly (of strength f) with the plasmon mode in the near-field of the MNP. This way, the MNP-QE dimer creates a Fano resonance effect on the SHG process, which takes place along the entire crystal body.

B. Analytical model

We first study the coupled system of the nonlinear crystal and the MNP-QE dimer with a basic analytical model. We obtain a simple analytical expression for the second-harmonic (SH) field amplitude α_2.

The equations of motion [Eqs. (A6a)–(A6e) in the Appendix] governing the dynamics of the system can be obtained from the Hamiltonian [Eq. (A5)] describing the system. One also includes the decay rates for the fields and the QE into the equations of motion. Derivations can be found in the Appendix.

In the steady state, the SH field amplitude α_2 can be obtained as

$$\alpha_2 = \frac{-i\chi_2}{[i(\Omega_2 - 2\omega) + \gamma_2] + \frac{|g|^2}{[i(\Omega_p - 2\omega) + \gamma_p] - \frac{|f|^2 y}{i(\omega_{\mathrm{QE}} - 2\omega) + \gamma_{\mathrm{QE}}}}} \alpha_1^2. \quad (1)$$

Here, $|\alpha_2|^2$ gives the number of SH-generated 2ω photons in the crystal. Similarly, $|\alpha_1|^2$ is the number of fundamental frequency (FF, ω) photons in the crystal. χ_2 is a constant (an overlap integral [38]) proportional to the second-order susceptibility of the nonlinear crystal, i.e., $\chi_2 \propto d_2$. $y = \rho_{ee} - \rho_{gg}$ is the population inversion of the QE, where ρ_{ee} and ρ_{gg} are the probabilities for the QE to be in the excited and the ground state, respectively, with the constraint $\rho_{ee} + \rho_{gg} = 1$. $\gamma_{1,2}$, γ_p, and γ_{QE} are the decay rates for the two crystal modes, namely the plasmon mode and the QE, respectively. $\Omega_{1,2}$, Ω_p, and ω_{QE} are the resonances in the same order.

1. Fano enhancement

Equation (1) reveals a striking mechanism for the Fano enhancement. Namely, one can increase the number of SH-generated photons $|\alpha_2|^2$ "without" increasing the number of photons in the FF ω, $|\alpha_1|^2$. This can simply be performed by introducing cancellations in the denominator of Eq. (1).

On the one hand, $|\alpha_2|^2$ can be enhanced via enhancing the first-harmonic field $|\alpha_1|^2$ using field-trapping techniques [24–29,31]. One increases $|\alpha_1|^2$, for instance, by using an ENZ material. On the other hand, the enhancement due to the cancellations in the denominator of Eq. (1) "multiplies" the enhancement of the $|\alpha_1|^2$. The latter enhancement (due to the denominator) is called the Fano enhancement. We state in advance that in our numerical simulations using the analytical model, $|\alpha_1|^2$ does not change, thus the enhancement in $|\alpha_2|^2$ originates solely from the denominator of Eq. (1). The number of photons in the α_2-mode is always (substantially) smaller than the number of photons of the FF α_1-mode.

The cancellation scheme works as follows. The first term in the denominator, $i(\Omega_2 - 2\omega) + \gamma_2$, belongs to the bare crystal. That is, only this term exists if the nonlinear crystal is not embedded with a MNP-QE dimer. The second term in the denominator, $|g|^2/(\cdots)$, appears due to the MNP-QE dimer. If one arranges g, f, ω_{QE} appropriately, the $|g|^2/(\cdots)$ term is able to cancel the first term partially. This can reduce the denominator in Eq. (1), thus enhancing the production of the SH 2ω photons $|\alpha_2|^2$ without relying on an enhancement in $|\alpha_1|^2$.

In Fig. 2, we present the enhancement that takes place merely due to the Fano resonance. We keep the laser (pump) strength constant and record the enhancement in $|\alpha_2|^2$. We observe that the SH intensity $|\alpha_2|^2$ can enhance $\sim$1000 times while the FF intensity $|\alpha_1|^2$ does not change. We calculate the amplitudes $\alpha_{1,2}$ via time evolution of the equations of motion for the system; see Eqs. (A6a)–(A6e) in the Appendix.

Throughout the paper, we scale frequencies by the constant Ω, the frequency of the 1064 nm light, i.e., $\Omega = 2\pi c/\Lambda$ with $\Lambda = 1064$ nm. In Fig. 2(a), we set the laser (pump) frequency to $\omega = \Omega$ (1064 nm) and vary the level spacing of the QE, ω_{QE}. We observe that for the choice of $\omega_{\mathrm{QE}} = \omega_{\mathrm{QE}}^{\star} \simeq 1.98\Omega$, the number of SH photons $|\alpha_2|^2$ is Fano-enhanced $\sim$2000 times via cancellations in the denominator of Eq. (1). (We use the star symbol $\star$ to indicate a value where the maximum/optimum enhancement is achieved.) $|\alpha_1|^2$ does not change (not depicted). In Fig. 2(b), we fix the QE level spacing to $\omega_{\mathrm{QE}} = 2\Omega$ and this time vary the frequency of the pump laser ω. We observe that for the pump frequency $\omega = \omega^{\star} \simeq 1.01\Omega$, the SHG $|\alpha_2|^2$ is Fano-enhanced $\sim$1500 times without increasing the FF field intensity $|\alpha_1|^2$.

In Fig. 2, we use the parameter set $\Omega_p = 1.77\Omega$, $\gamma_p = 0.1\Omega$, $g = f = 0.1\Omega$, $\Omega_1 = 1.007\Omega$, $\Omega_2 = 2.013\Omega$, $\gamma_{1,2} = 0.005\Omega$, and $\chi_2 = 10^{-4}\Omega$ (e.g., a small converter). The particular value of χ_2 does not change the enhancement factors in our simulations. In Fig. 2(a) we set $\omega = \Omega$. In Fig. 2(b) we set $\omega_{\mathrm{QE}} = 2\Omega$. These parameters are chosen according to the numerical simulations we conduct in the following section. For instance, the resonance frequency of the MNP Ω_p is set to $\lambda_p = 600$ nm ($\Omega_p = 2\pi c/\lambda_p$). This is the resonance frequency of the gold NP plasmon calculated in an

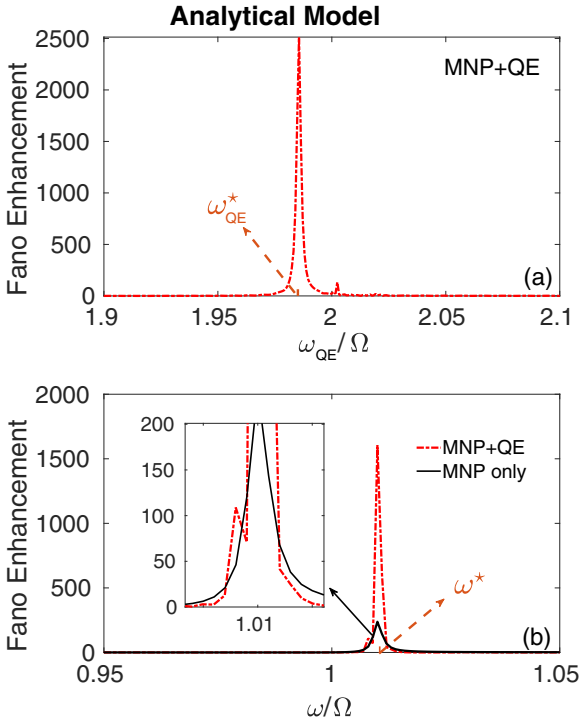

FIG. 2. Fano enhancement factors predicted by the analytical model. (a) We scan different values of the QE level spacing $\omega_{\rm QE}$ in order to find the particular value $\omega^\star_{\rm QE} \simeq 1.98\Omega$ which performs cancellations in the denominator of α_2 in Eq. (1). The Fano enhancement factor reaches ∼2500. (b) We also fix the QE at $\omega_{\rm QE} = 2\Omega$ and scan the pump frequency ω in order to find the particular value $\omega^\star = 1.01\Omega$ which performs cancellations in the denominator of α_2 in Eq. (1). The MNP-QE dimer (red dashed line) can achieve a Fano enhancement factor of ∼1500. Using only MNPs (black line) can also introduce a Fano enhancement factor of ∼200. The FF field $|\alpha_1|^2$ does not change (not depicted). The frequencies are scaled with the frequency of the $\Lambda = 1064$ nm light, i.e., $\Omega = 2\pi c/1064$ nm.

$n_{\rm KDP} = 1.51$ index medium using the experimental dielectric function of gold [35]. The decay rates are chosen close to the ones for the crystal, plasmon, and QE linewidths. We keep the parameters close to the ones for the numerical simulations, because we aim at a *basic* comparison between the analytical and numerical (Maxwell) solutions. That is, we aim to check if the Fano enhancement appears using similar parameters in the analytical and the numerical simulations. In the next section, we show that an excellent agreement occurs between the two results.

We can state the usefulness of the analytical model as follows. In a numerical (Maxwell) simulation alone, it is not possible to differentiate between a Fano enhancement and an enhancement due to local field improvement. Our analytical treatment sheds light on the numerical results. This is because the analytical model does not take the localization effects (e.g., the change in the density of states near a MNP) into account. Thus, the enhancement factors presented by the analytical model are only due to the Fano enhancement. This provides a useful tool in understanding the origins of the SHG enhancement. One can appreciate this better in the treatment below, where a MNP is shown to give rise to Fano enhancement without a QE. We also demonstrate this phenomenon using numerical simulations.

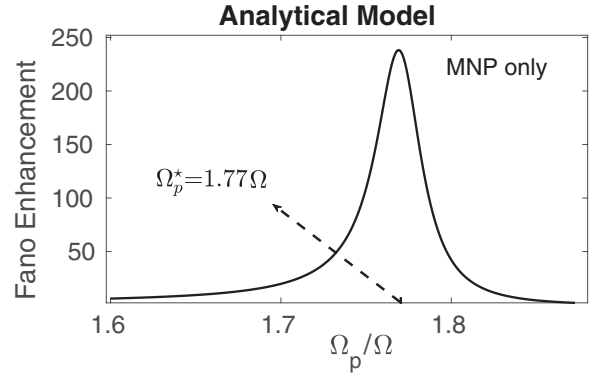

FIG. 3. Fano enhancement can also be achieved using only MNPs. We scan the plasmon resonance Ω_p of the MNP in order to find the particular value $\Omega_p^\star \simeq 1.77\Omega$ where cancellations in the denominator of α_2 take place; see Eq. (2).

The presented analytical model is also valid (even to a higher extent) when the MNP-QE dimers are placed on the surface of the nonlinear crystal. In this case, MNP couples with the evanescent waves of the α_2 mode. Strong coupling between the evanescent waves and the metal nanostructures decorated on the crystals is a well-reported phenomenon [39–42].

We further observe that the interference scheme (i.e., the cancellations in the denominator) for the Fano control of an unlocalized system is different from the one for the localized nonlinear processes. In the Fano control of a local process (when the nonlinear process takes place at the hot spot), the denominator contains only the $[i(\Omega_2 - 2\omega) + \gamma_2] - \frac{|f|^2 y}{i(\omega_{\rm QE} - 2\omega) + \gamma_{\rm QE}}$ term [21]. In Eq. (1), we observe that the cancellation scheme is richer.

In brief, in Fig. 5, approximately a 2 times SHG enhancement appears due to the local field enhancement caused by the MNP resonance near the converted frequency 2ω; see Fig. S5 in Ref. [35]. The remaining enhancement takes place due to the Fano enhancement factor as local field enhancement does not appear at ω; see Fig. S4.

2. Fano enhancement using only MNPs

A MNP is a strongly absorbing material with a broad linewidth. However, the analytical model below shows that a MNP alone can also introduce Fano enhancement effects. To study this phenomenon, we simply set the MNP-QE coupling to zero in Eq. (1), i.e., $f = 0$, and obtain the SH amplitude

$$\alpha_2 = \frac{-i\chi_2}{[i(\Omega_2 - 2\omega) + \gamma_2] + \frac{|g|^2}{[i(\Omega_p - 2\omega) + \gamma_p]}} \alpha_1^2. \qquad (2)$$

Here, the $|g|^2/(\cdots)$ term can perform cancellations in the (first) term belonging to the bare crystal. The cancellation can be performed for the proper choices of Ω_p, $|g|^2$, and ω. In Fig. 2(b), we demonstrate the phenomenon by varying the pump frequency ω for a fixed $\Omega_p = 1.773\Omega$ (600 nm) and $g = 0.1\Omega$. The black line shows a 200 Fano enhancement factor. In Fig. 3, the pump frequency is fixed at $\omega = \Omega$ and the

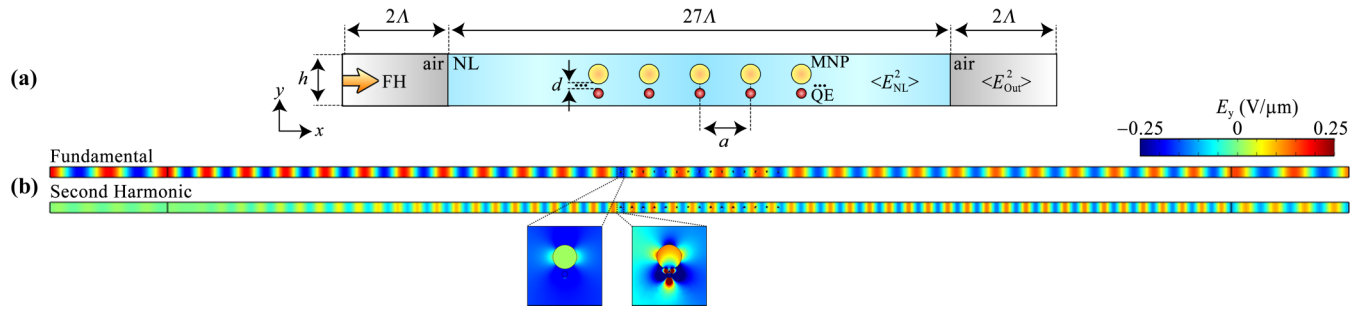

FIG. 4. A sketch of the computational domain employed in FEM simulations. (a) A 27 × 1064 nm long nonlinear (KDP) crystal is embedded with MNP-QE dimers of diameters 20 and 5 nm, respectively. The MNP and QE has a surface-to-surface distance of $d = 2$ nm and the dimers are separated by $a = 200$ nm in the x-direction. The E-field of the pump laser is chosen along the y-direction, thus the hot spot of the MNP is located at the position where the QE is placed. We use the experimental dielectric functions of the materials and a Lorentzian for the QE. (b) Close-up views of the FF and the SH field distributions. See Ref. [35] for further details.

MNP resonance exhibits an ∼200 times Fano enhancement at $\Omega_p = \Omega_p^\star = 1.77\Omega$, with $g = 0.1\Omega$. In Figs. 2 and 3, the strength of the laser pump and the FF intensity $|\alpha_1|^2$ do not change. We confirm this phenomenon with the numerical solutions of Maxwell's equations in the next section.

C. Numerical solutions of Maxwell's equations

In the previous section, we anticipated the presence of a three-orders-of-magnitude Fano enhancement from our analytical model. In this section, we check the phenomenon with the numerical simulations of Maxwell's equations, and we compare the two results.

We solve Maxwell's equations for the system presented in Fig. 4(a) using the finite-element method (FEM). We perform the calculations in COMSOL MULTIPHYSICS [34]. We consider a KDP nonlinear crystal for the SHG process. It has a refractive index of $n_{\text{KDP}} = 1.51$ and a second-order nonlinear coefficient of $d_2 = 10^{-18}$ C/V^2. The length of the KDP crystal is chosen as 27 × 1064 nm. We consider a width $h = 200$ nm for the KDP in our simulations. The horizontal (y-direction) boundaries are paired by Bloch-Floquet boundary conditions.

The MNP-QE dimers embedded into the crystal have diameters of 20 and 5 nm, respectively. The distance between the MNP and QE is $d = 2$ nm. The separation between the adjacent dimers is $a = 200$ nm along the x-direction. We use the experimental dielectric functions for the KDP and the gold NP, and a Lorentzian dielectric function for the QE [15]. The linewidth of the QE is set as $\gamma_{\text{QE}} = 5 \times 10^{11}$ Hz. The QE has an oscillator strength of $f_{\text{osc}} = 0.1$ and the permittivity constant is set to $\epsilon_\infty = 1$.

We pump the system with a laser of intensity $I_0 = 100$ MW/m^2. The wavelength of the pump is fixed at $\lambda = 1064$ nm ($\omega = 2\pi c/\lambda$) in Fig. 5(a), but varied in Fig. 5(b). As in the analytical treatment, we scale frequencies by the frequency corresponding to the 1064 nm laser, i.e., $\Omega = 2\pi c/\Lambda$ with $\Lambda = 1064$ nm. Hence, in Fig. 5(a) the laser frequency is set to $\omega = 1 \times \Omega$. Details about the computations can be found in Ref. [35].

1. Fano enhancement

We calculate the SH field at (i) the output, (ii) along the crystal body, and (iii) at the hot spots between the MNP and the QE; see Fig. 4(a). Simulations produce interesting results.

In Fig. 5, we plot the total SH enhancement at the "output" of the KDP crystal, i.e., at the air region on the right in Fig. 4(a). We compare the SH intensities with and without the presence of the MNP-QE dimers. In Fig. 5(a), we fix the pump frequency to $\omega = \Omega$, and we seek the optimum value of the QE level spacing $\omega_{\text{QE}}^\star$ at which we obtain an appreciable enhancement. At $\omega_{\text{QE}} = \omega_{\text{QE}}^\star \simeq 1.98\Omega$, an ∼1000 times SHG enhancement at the KDP output can be observed. In contrast with such a total enhancement, the average SH field inside the crystal is suppressed to 70% of the one for the bare crystal (without the MNP-QE dimers). The SH intensity in the crystal is enhanced only at the hot spot between the MNP and the QE. But this is only a 2 times enhancement, and it takes place only in a small region. Moreover, the FF ω intensity inside the crystal is 95% of that for the bare crystal.

Therefore, the ∼1000 times total enhancement at the crystal output cannot originate from the localization (field-trapping) type enhancement employed in other studies [24–29,31]. Then, the observed SHG enhancement is the Fano enhancement that our analytical model predicts in Fig. 2(a). Furthermore, the Fano enhancement in the analytical model and the numerical simulations appears at the same QE level spacing $\omega_{\text{QE}} = \omega_{\text{QE}}^\star \simeq 1.98\Omega$. We make an effort to use similar parameters in the analytical and numerical treatments. For instance, the resonances $\Omega_1 \simeq 1.007\Omega$ (FF mode) and $\Omega_2 \simeq 2.013\Omega$ (SH mode), which we use in the analytical model, are chosen by rough calculations for the KDP crystal depicted in Fig. 4(a). Our purpose in conducting the numerical simulations is only to demonstrate the presence of the Fano enhancement in the SHG process, in the absence of field trapping.

We also compare the analytical and numerical results for a varying laser (pump) frequency ω at the fixed QE level spacing $\omega_{\text{QE}} = 2\Omega$. Figure 5(b) shows that an ∼1500 times total SHG enhancement appears at the "output" of the nonlinear crystal. This enhancement is attained at the pump frequency $\omega = \omega^\star = 1.015\Omega$ ($\lambda^\star = 1048$ nm). Please note that the enhancement peak at $\omega = \omega^\star = 1.01\Omega$ [Fig. 2(b)], in the analytical treatment, shows an excellent agreement with the numerical results. Additionally, both Figs. 5(b) and 2(b) display a shouldered curve as a common aspect.

The average SH intensity in the crystal body drops to 90% of that for the bare crystal. The SH intensity increases only

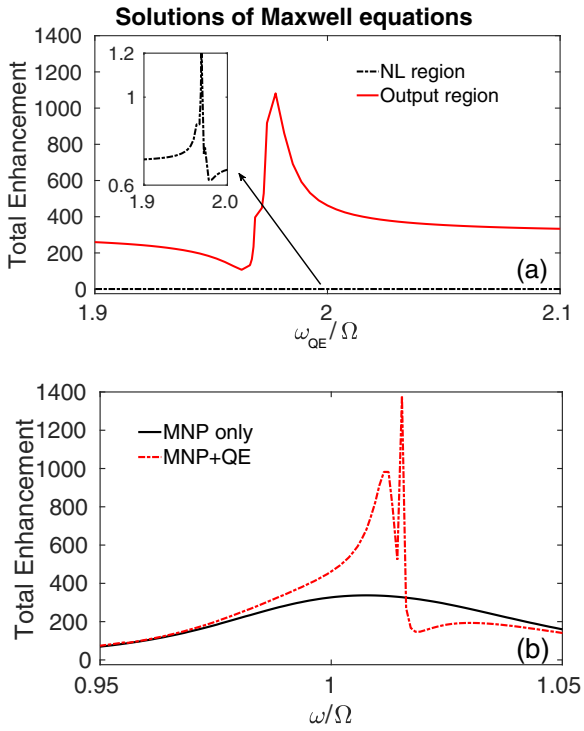

FIG. 5. Numerical solutions of Maxwell's equations. Total enhancement factors (EFs) for the SH intensity, calculated at the crystal output, when MNP-QE dimers are placed into the crystal; see Fig. 4. As the FF (ω) intensity is not enhanced in the crystal, the plotted total EFs correspond to the Fano enhancement; see the text. (a) Like in the analytical model, Fig. 2(a), we scan the QE level spacing ω_{QE}. An ∼1000 SH intensity enhancement takes place at $\omega_{QE} = \omega^{\star}_{QE} \simeq 1.98\Omega$, which is similar to the analytical result in Fig. 2(a). (b) We fix the $\omega_{QE} = 2\Omega$, as in Fig. 2(b), and scan the pump frequency ω. An ∼1400 enhancement factor appears (red dashed line) at $\omega = \omega^{\star} = 1.015\Omega$, which is close to the one predicted by the analytical model in Fig. 2(b). Fano enhancement also takes place using only MNPs (black line) as the analytical model predicts in Fig. 2(b) (black line). The local fields are not enhanced. In (a) and (b), an approximately 2 times enhancement appears due to the local field enhancement of the MNP resonance, near 2ω (Figs. S4 and S5). The remaining enhancement originates from the Fano enhancement.

2 times at the small region, i.e., at the hot spot between the MNP and the QE. Moreover, the FF ω field is suppressed to 56% of the bare crystal. The localized field enhancement is not sufficient to account for the SHG enhancement alone. Thus, the ∼1500 times total enhancement at the output can only be explained by the unlocalized Fano enhancement factor, as we suggest.

In our FEM simulations, the dimers are placed periodically ($a = 200$ nm) along the x-direction. We also checked if any effect due to periodicity intervenes with the Fano enhancement profile in Fig. 5. We performed control simulations also for different distances between the dimers other than $a = 200$ nm. The enhancement factors remained almost unaltered.

2. Fano enhancement using only MNPs

We also carry out FEM simulations for a KDP crystal embedded only with MNPs. We confirm the Fano enhancement effect predicted by the analytical model in Eq. (2). In Fig. 5(b), black line, we observe that the total SH intensity at the crystal output is enhanced about 300 times using only MNPs. This enhancement takes place in spite of the fact that both FF and SH fields inside the crystal do not intensify. That is, the 300 times total enhancement cannot be explained with the localization effects, thus it is chiefly due to the Fano enhancement effect. Comparing the black lines in Figs. 5(b) and 2(b), one can observe that the Fano enhancement appears at similar locations. A comparison with Fig. 3 cannot be performed since the actual (experimental) dielectric function for the gold NP is used.

As a final remark, the resonance of the MNPs—that we use in all of the analytical and numerical simulations—is set around the SH 2ω field. That is, one already should not expect a localization effect in the fundamental (ω) field. The localization in the SH field—only at the hot spots—is at most 2 times in all of the FEM simulations, thus it cannot explain the three order enhancements at the crystal output. We remind the reader that the average SH intensity inside the crystal even reduces compared to a bare crystal.

III. DISCUSSION

We demonstrate the Fano control of unlocalized nonlinear processes that take place throughout an entire crystal body. MNP-QE dimers interact with the converted crystal field and introduce Fano resonances. The dimers can either be embedded into the crystal or they can be placed on the crystal surface. A three-orders-of-magnitude Fano enhancement takes place for the appropriate choice of the QE's level spacing, ω_{QE}. We demonstrate the phenomenon both on a basic analytical model and via FEM-based numerical solutions of Maxwell's equations.

The analytical model predicts the presence of such a Fano enhancement, and the FEM simulations confirm its existence. The analytical model yields a simple expression for the SH field amplitude; see Eq. (1). The mechanism of the enhancement can be explained by this simple statement: the cancellations in the denominator result in the Fano enhancement. This expression also shows why the Fano enhancement multiplies the enhancements due to field-trapping techniques [24–29,31].

The FEM simulations demonstrate the Fano enhancement predicted by the analytical model. The crystal output field (in total) is enhanced by three orders, while the linear and nonlinear fields inside the crystal are not enhanced. Thus, the three-orders-of-magnitude total enhancement is proven to originate from the Fano enhancement. Moreover, the frequency dependence of the Fano enhancement factors displays good agreement between the analytical and the FEM results.

The Fano enhancement scheme we develop is outstanding, because (i) it multiplies ($\sim 10^3\times$) the enhancements achieved via field-trapping techniques, (ii) an applied voltage can continuously tune the Fano resonances, and (iii) it has on-chip implementations, where miniaturization and energy efficiency are very important. Moreover, (iv) the extra (Fano) enhancement scheme works equally for other nonlinear processes [35].

The Fano enhancement scheme can be used together with any of the field-trapping techniques. It multiplies the enhancements achieved by ENZ materials [26–29,31] or nanoparticle doping [24,25] by a factor of $\sim 10^3$. ENZ compatibility of the method has particular importance for relatively longer (>10 μm) photonic devices. This is because ENZ materials relieve the phase-matching conditions substantially [30], thus they are unrivaled for the efficient operation of nonlinear devices longer than ~ 10 μm [30].

The level spacing of a QE can be tuned via an applied voltage [43], thus one can continuously switch between different Fano enhancement factors in Figs. 2(a) and 5(a). Fano enhancements appear at sharp resonances. Roughly an 8–10 meV voltage tuning [44] corresponds to an arrangement of the Fano enhancement factor between 100 and 1000.

The demonstrated unlocalized Fano enhancement scheme is quite important in on-chip implementations with nano/microscale devices. As the Fano enhancement multiplies the nonlinear signal by a factor of $\sim$1000, the same nonlinearity can be obtained using an $I_0/\sqrt{1000} \simeq I_0/33$ power input instead of I_0. This implies a significantly lower energy consumption in a chip element. Additionally, similar nonlinear conversion rates can be achieved at substantially smaller lengths, which helps the miniaturization of such chip elements. The presented enhancement scheme targets the implementations in relatively small (nano/microscale, integrable) devices where nonlinearity generation is quite low.

We note that the Fano enhancement scheme employing the MNP-QE dimers is limited by the saturation of the QEs. When the QEs become saturated, population inversion y approaches zero in Eq. (1). Thus, path interference due to the QEs cannot take place. We calculate the saturation limit as about $\sim$6 SH (2ω) photons per QE; see the Appendix. When N number of dimers each having M number of defect-centers (e.g., a 2D material or a nanodiamond with silicon-vacancy defect centers [45]) are used, the saturation limit for the SH-generated photons becomes about $\sim N \times M \times 6$. M can be as large as 30 in a nanodiamond of 5 nm size. That is, Fano enhancement can increase the $0.006 \times N \times M$ number of 2ω photons to $6 \times N \times M$, but it cannot raise the $6 \times N \times M$ photons to $6000 \times N \times M$, assuming a 1000 times enhancement. Using a single MNP-QE dimer, the limit $M \times 6$ is sufficient for nano/microscale quantum optics/plasmonics applications where energy efficiency and voltage-tunability is important. However, for large nonlinear crystal converters, the method is inadequate because decorating them with MNP-QE dimers is not efficient. Nevertheless, MNP-only Fano enhancement (Fig. 3) is not limited by the QE saturation. So, the MNP-QE Fano enhancement scheme becomes an intensity-dependent phenomenon at high conversion intensities. Still, the voltage-tunable Fano enhancement is attractive in nano/microdevices due to the voltage control and about 33 times the energy efficiency.

In the paper, we only work on the Fano enhancement of the SHG process. The Fano enhancement scheme that we demonstrate, however, can also be used in other nonlinear processes. In Ref. [35], we show that Fano enhancement schemes, similar to Eq. (1), appear also for third-harmonic generation and the four-wave mixing processes. Similarly, Fano enhancement further multiplies the enhancements achieved by field-trapping techniques in higher-order nonlinearities.

ACKNOWLEDGMENTS

We thank the referee for comments and suggestions on including the analysis for the saturation effect. M.G. and M.E.T. are supported by TUBITAK-1001 under Grant No. 117F118. A.B. and M.E.T. are supported by TUBITAK-1001 under Grant No. 119F101. M.E.T. and A.C. acknowledge support from Turkish Academy of Sciences (TUBA) Outstanding Young Researchers Awarding Programme (GEBIP).

APPENDIX

1. Derivation of the Fano enhancement

In this Appendix, we obtain the equations of motion (EOMs) for the dynamics of a nonlinear crystal coupled to a MNP-QE dimer.

The components of the Hamiltonian for the coupled system can be expressed as follows. The occupation energies of the crystal modes (α_1, α_2), the plasmon mode (α_p), and the excitation of the QE can be written as

$$\hat{\mathcal{H}}_0 = \hbar\Omega_1 \hat{a}_1^\dagger \hat{a}_1 + \hbar\Omega_2 \hat{a}_2^\dagger \hat{a}_2 + \hbar\Omega_p \hat{a}_p^\dagger \hat{a}_p + \hbar\omega_{eg} |e\rangle\langle e|,$$

where $\hat{a}_{1,2}^\dagger$ ($\hat{a}_{1,2}$) creates (annihilates) a photon in the $\alpha_{1,2}$-modes of the nonlinear crystal. Similarly, $\hat{a}_p^\dagger$ ($\hat{a}_p$) creates (annihilates) a plasmon in the α_p-mode of the MNP. The field profile of the MNP's plasmon mode displays a localization at its hot spot. $|e\rangle$ stands for the excited state, and the operator $|e\rangle\langle e|$ determines the probability of the QE to be in the excited state. $\hat{a}_i^\dagger \hat{a}_i$, $i = 1, 2, p$, determines the number of photons (plasmons) in the modes.

The α_1-mode of the crystal is pumped,

$$\hat{\mathcal{H}}_{\text{L}} = i\hbar(\varepsilon_{\text{L}} \hat{a}_1^\dagger e^{-i\omega t} - \text{H.c.}), \tag{A1}$$

by a laser of frequency ω. Thus, ω frequency photons are created ($\hat{a}_1^\dagger$) in the α_1-mode. ε_{L} is proportional to the laser field amplitude, and H.c. denotes Hermitian conjugate. The crystal performs SHG: two ω photons in the α_1-mode annihilate ($\hat{a}_1^2$), and a 2ω photon is created in the ($\hat{a}_2^\dagger$) α_2-mode,

$$\hat{\mathcal{H}}_{\text{SH}} = \hbar\chi_2(\hat{a}_2^\dagger \hat{a}_1 \hat{a}_1 + \text{H.c.}). \tag{A2}$$

The converted (2ω) field couples with the plasmon mode of the MNP,

$$\hat{\mathcal{H}}_g = \hbar g(\hat{a}_p^\dagger \hat{a}_2 + \text{H.c.}), \tag{A3}$$

where a photon in the α_2-mode annihilates ($\hat{a}_2$) and creates a plasmon ($\hat{a}_p^\dagger$) on the MNP (α_p-mode). The plasmon mode profile displays a hot spot. The QE placed at the hot spot interacts strongly with the plasmon field. A plasmon can annihilate ($\hat{a}_p$) and excite the QE to the upper level ($|e\rangle\langle g|$),

$$\hat{\mathcal{H}}_{\text{int}} = \hbar f(|e\rangle\langle g| \hat{a}_p + \text{H.c.}). \tag{A4}$$

Thus, the total Hamiltonian can be written as

$$\hat{\mathcal{H}} = \hat{\mathcal{H}}_0 + \hat{\mathcal{H}}_{\text{L}} + \hat{\mathcal{H}}_{\text{SH}} + \hat{\mathcal{H}}_g + \hat{\mathcal{H}}_{\text{int}}. \tag{A5}$$

The set of EOMs for this system can be obtained using the Heisenberg EOM, e.g., $i\hbar\dot{a} = [\hat{a}_i, \hat{\mathcal{H}}]$, where $i = 1, 2, p$. For

investigating only the field amplitudes, the second-quantized operators can be replaced by their expectations, e.g., $\alpha_i = \langle \hat{a}_i \rangle$. We also replace $\hat{\rho}_{ij} = |i\rangle\langle j| \to \rho_{ij}$ [46]. Including also the decay rates for the fields and the QE, the EOM can be obtained as

$$\dot{\alpha_1} = -(i\Omega_1 + \gamma_1)\alpha_1 - i2\chi_2\alpha_1^*\alpha_2 + \varepsilon_L e^{-i\omega t}, \quad \text{(A6a)}$$

$$\dot{\alpha_2} = -(i\Omega_2 + \gamma_2)\alpha_2 - i\chi_2\alpha_1^2 - ig\alpha_p, \quad \text{(A6b)}$$

$$\dot{\alpha_p} = -(i\Omega_p + \gamma_p)\alpha_p - ig\alpha_2 - if\rho_{ge}, \quad \text{(A6c)}$$

$$\dot{\rho}_{ge} = -(i\omega_{eg} + \gamma_{eg})\rho_{ge} + if\alpha_p(\rho_{ee} - \rho_{gg}), \quad \text{(A6d)}$$

$$\dot{\rho}_{ee} = -\gamma_{ee}\rho_{ee} + i(f\rho_{ge}\alpha_p^* - \text{c.c.}), \quad \text{(A6e)}$$

where γ_i stands for the decay rates, and $\gamma_{eg} = \gamma_{ee}/2$. In the text, we use $\gamma_{QE} \equiv \gamma_{eg}$ for simplicity.

The system is driven by a source oscillating as $\sim e^{-i\omega t}$. Investigating Eqs. (A6a)–(A6e), one can see that the solutions at the steady state oscillate as $\alpha_1(t) = \tilde{\alpha}_1 e^{-i\omega t}$, $\alpha_{2,p}(t) = \tilde{\alpha}_{2,p} e^{-i2\omega t}$, and $\rho_{ge}(t) = \tilde{\rho}_{ge} e^{-i2\omega t}$, where the terms with the tilde are constants that determine the steady-state field amplitudes. We put these solutions into the EOM (A6a)–(A6e) and obtain the equations

$$0 = -[i(\Omega_1 - \omega) + \gamma_1]\tilde{\alpha}_1 - i2\chi_2\tilde{\alpha}_1^*\tilde{\alpha}_2 + \varepsilon_L, \quad \text{(A7a)}$$

$$0 = -[i(\Omega_2 - 2\omega) + \gamma_2]\tilde{\alpha}_2 - i\chi_2\tilde{\alpha}_1^2 - ig\tilde{\alpha}_p, \quad \text{(A7b)}$$

$$0 = -[i(\Omega_p - 2\omega) + \gamma_p]\tilde{\alpha}_p - ig\tilde{\alpha}_2 - if\tilde{\rho}_{ge}, \quad \text{(A7c)}$$

$$0 = -[i(\omega_{eg} - 2\omega) + \gamma_{eg}]\tilde{\rho}_{ge} + if\tilde{\alpha}_p(\rho_{ee} - \rho_{gg}), \quad \text{(A7d)}$$

$$0 = -\gamma_{ee}\rho_{ee} + i(f\tilde{\rho}_{ge}\tilde{\alpha}_p^* - f^*\tilde{\rho}_{ge}^*\tilde{\alpha}_p) \quad \text{(A7e)}$$

for the steady-state values. The equations for the steady-state amplitudes are not exactly solvable. However, one can still express the SH field amplitude $\tilde{\alpha}_2$ as in Eq. (1) using Eqs. (A7b)–(A7d). This solution, i.e., Eq. (1), provides us with an invaluable insight for the Fano enhancement and its relation to the enhancements obtained via field-trapping techniques. In the text, in Eqs. (1) and (2), we drop the tilde symbols for the sake of simplicity.

2. Saturation limit

The Fano enhancement scheme is dependent on the intensity (number) of the converted SH photons. This is because when the plasmon mode (into which the QE is coupled) is strongly excited by the α_2 photons, a "single QE" can reach the saturation limit. This makes the population inversion $y = \rho_{ee} - \rho_{gg}$ approach zero in the denominator of Eq. (1) where interference due to the QE may not be possible. The MNP-only Fano enhancement (Fig. 3) is not affected by the QE saturation. We can obtain an approximate limit for the SH conversion (per QE), before the saturation, as follows. When we use Eq. (A7d) in Eq. (A7e), we obtain an equation for the excited-state population,

$$\rho_{ee} = \frac{|\alpha_p|^2}{\gamma_{ee}}(\rho_{ee} - \rho_{gg})G(\omega), \quad \text{(A8)}$$

where

$$G(\omega) = 2\frac{\gamma_{eg}\text{Re}(f^2) + (\omega_{eg} - 2\omega)\text{Im}(f^2)}{(\omega_{eg} - 2\omega)^2 + \gamma_{eg}^2}. \quad \text{(A9)}$$

Using $\rho_{ee} + \rho_{gg} = 1$ and solving Eq. (A8) for ρ_{ee}, we find that

$$\rho_{ee} = \frac{|\alpha_p|^2 G(\omega)/\gamma_{ee}}{1 + 2|\alpha_p|^2 G(\omega)/\gamma_{ee}}. \quad \text{(A10)}$$

Thus, approximately for

$$|\alpha_p|^2 G(\omega)/\gamma_{ee} \gtrsim 1 \quad \text{(A11)}$$

the single QE reaches the saturation limit. Using Eq. (A7b), we approximately obtain the SH conversion limit as $|\alpha_2|^2 \sim 6$ photons per QE for the parameters we use in Fig. 2.

For many nano/microscale quantum optics/plasmonics applications, such a nonlinearity is quite sufficient where a nano/microscale converter works with, e.g., ∼33 times the efficiency. Still, one can increase the number of generated photons M times by using M defect-centers in a single MNP-QE dimer. In this case, once can show [using Eqs. (A7a)–(A7e)] that the saturation limit increases M times. M can be as large as 30 nanodiamonds of 5 nm size. Moreover, for a relatively larger converter (e.g., more than a few microns), the conversion limit can be increased many times by using N number of such dimers. The new SH converted photon limit becomes, e.g., $\sim 6 \times M \times N$. Thus, the MNP-QE Fano enhancement scheme is useful especially for nano/microscale devices. Decorating the macroscopic nonlinear crystal converters with MNP-QE dimers is naturally not an efficient method.

[1] M. S. Tame, K. R. McEnery, Ş. Özdemir, J. Lee, S. A. Maier, and M. S. Kim, Quantum plasmonics, Nat. Phys. **9**, 329 (2013).

[2] M. I. Stockman, Nanoplasmonics: Past, present, and glimpse into future, Opt. Express **19**, 22029 (2011).

[3] C. Höppener, Z. J. Lapin, P. Bharadwaj, and L. Novotny, Self-Similar Gold-Nanoparticle Antennas for a Cascaded Enhancement of the Optical Field, Phys. Rev. Lett. **109**, 017402 (2012).

[4] J. N. Anker, W. Hall, O. Lyandres, N. C. Shah, J. Zhao, and R. P. Van Duyne, Biosensing with plasmonic nanosensors, Nat. Mater. **7**, 442 (2008).

[5] A. Lewis, H. Taha, A. Strinkovski, A. Manevitch, A. Khatchatouriants, R. Dekhter, and E. Ammann, Near-field optics: from subwavelength illumination to nanometric shadowing, Nat. Biotechnol. **21**, 1378 (2003).

[6] R. Zhang, Y. Zhang, Z. C. Dong, S. Jiang, C. Zhang, L. G. Chen, L. Zhang, Y. Liao, J. Aizpurua, Y. Luo *et al.*, Chemical mapping of a single molecule by plasmon-enhanced Raman scattering, Nature (London) **498**, 82 (2013).

[7] V. Giannini, A. I. Fernández-Domínguez, S. C. Heck, and S. A. Maier, Plasmonic nanoantennas: Fundamentals and their use in controlling the radiative properties of nanoemitters, Chem. Rev. **111**, 3888 (2011).

[8] M. Kauranen and A. V. Zayats, Nonlinear plasmonics, Nat. Photon. **6**, 737 (2012).

[9] N. Weber, M. Protte, F. Walter, P. Georgi, T. Zentgraf, and C. Meier, Double resonant plasmonic nanoantennas for efficient

second harmonic generation in zinc oxide, Phys. Rev. B **95**, 205307 (2017).

[10] J. Ye, F. Wen, H. Sobhani, J. B. Lassiter, P. Van Dorpe, P. Nordlander, and N. J. Halas, Plasmonic nanoclusters: Near field properties of the Fano resonance interrogated with SERS, Nano Lett. **12**, 1660 (2012).

[11] Y. Chu, M. G. Banaee, and K. B. Crozier, Double-resonance plasmon substrates for surface-enhanced Raman scattering with enhancement at excitation and Stokes frequencies, ACS Nano **4**, 2804 (2010).

[12] M. Pelton, S. D. Storm, and H. Leng, Strong coupling of emitters to single plasmonic nanoparticles: Exciton-induced transparency and Rabi splitting, Nanoscale **11**, 14540 (2019).

[13] N. Liu, L. Langguth, T. Weiss, J. Kästel, M. Fleischhauer, T. Pfau, and H. Giessen, Plasmonic analogue of electromagnetically induced transparency at the Drude damping limit, Nat. Mater. **8**, 758 (2009).

[14] H. Leng, B. Szychowski, M.-C. Daniel, and M. Pelton, Strong coupling and induced transparency at room temperature with single quantum dots and gap plasmons, Nat. Commun. **9**(1), 4012 (2018).

[15] X. Wu, S. K. Gray, and M. Pelton, Quantum-dot-induced transparency in a nanoscale plasmonic resonator, Opt. Express **18**, 23633 (2010).

[16] S. Zhang, D. A. Genov, Y. Wang, M. Liu, and X. Zhang, Plasmon-Induced Transparency in Metamaterials, Phys. Rev. Lett. **101**, 047401 (2008).

[17] A. Panahpour, A. Mahmoodpoor, and A. V. Lavrinenko, Refraction enhancement in plasmonics by coherent control of plasmon resonances, Phys. Rev. B **100**, 075427 (2019).

[18] J. Butet and O. J. F. Martin, Fano resonances in the nonlinear optical response of coupled plasmonic nanostructures, Opt. Express **22**, 29693 (2014).

[19] K. Thyagarajan, J. Butet, and O. J. F. Martin, Augmenting second harmonic generation using Fano resonances in plasmonic systems, Nano Lett. **13**, 1847 (2013).

[20] J. Butet, G. Bachelier, I. Russier-Antoine, F. Bertorelle, A. Mosset, N. Lascoux, C. Jonin, E. Benichou, and P.-F. Brevet, Nonlinear Fano profiles in the optical second-harmonic generation from silver nanoparticles, Phys. Rev. B **86**, 075430 (2012).

[21] D. Turkpence, G. B. Akguc, A. Bek, and M. E. Tasgin, Engineering nonlinear response of nanomaterials using Fano resonances, J. Opt. **16**, 105009 (2014).

[22] E. Paspalakis, S. Evangelou, S. G. Kosionis, and A. F. Terzis, Strongly modified four-wave mixing in a coupled semiconductor quantum dot-metal nanoparticle system, J. Appl. Phys. **115**, 083106 (2014).

[23] S. K. Singh, M. K. Abak, and M. E. Tasgin, Enhancement of four-wave mixing via interference of multiple plasmonic conversion paths, Phys. Rev. B **93**, 035410 (2016).

[24] W. Nie, Y. Zhang, H. Yu, R. Li, R. He, N. Dong, J. Wang, R. Hübner, R. Böttger, S. Zhou *et al.*, Plasmonic nanoparticles embedded in single crystals synthesized by gold ion implantation for enhanced optical nonlinearity and efficient Q-switched lasing, Nanoscale **10**, 4228 (2018).

[25] R. Li, N. Dong, C. Cheng, F. Ren, R. Hübner, J. Wang, S. Zhou, and F. Chen, Giant enhancement of nonlinear optical response in Nd:YAG single crystals by embedded silver nanoparticles, ACS Omega **2**, 1279 (2017).

[26] O. Reshef, I. De Leon, M. Z. Alam, and R. W. Boyd, Nonlinear optical effects in epsilon-near-zero media, Nat. Rev. Mater. **4**, 535 (2019).

[27] A. Capretti, Y. Wang, N. Engheta, and L. Dal Negro, Comparative study of second-harmonic generation from epsilon-near-zero indium tin oxide and titanium nitride nanolayers excited in the near-infrared spectral range, ACS Photon. **2**, 1584 (2015).

[28] T. S. Luk, D. De Ceglia, S. Liu, G. A. Keeler, R. P. Prasankumar, M. A. Vincenti, M. Scalora, M. B Sinclair, and S. Campione, Enhanced third harmonic generation from the epsilon-near-zero modes of ultrathin films, Appl. Phys. Lett. **106**, 151103 (2015).

[29] J. Deng, Y. Tang, S. Chen, K. Li, A. V. Zayats, and G. Li, Giant enhancement of second-order nonlinearity of epsilon-near-zero medium by a plasmonic metasurface, Nano Lett. **20**, 5421 (2020).

[30] M. Kauranen, Freeing nonlinear optics from phase matching, Science **342**, 1182 (2013).

[31] M. A. Vincenti, M. Kamandi, D. de Ceglia, C. Guclu, M. Scalora, and F. Capolino, Second-harmonic generation in longitudinal epsilon-near-zero materials, Phys. Rev. B **96**, 045438 (2017).

[32] A. Ahmadivand, M. Semmlinger, L. Dong, B. Gerislioglu, P. Nordlander, and N. J. Halas, Toroidal dipole-enhanced third harmonic generation of deep ultraviolet light using plasmonic meta-atoms, Nano Lett. **19**, 605 (2018).

[33] D. N. Nikogosyan, *Nonlinear Optical Crystals: A Complete Survey* (Springer Science & Business Media, New York, NY, 2006).

[34] COMSOL multiphysics v. 5.4. https://www.comsol.com. COMSOL AB, Stockholm, Sweden.

[35] See Supplemental Material at http://link.aps.org/supplemental/10.1103/PhysRevB.104.235407 for a detailed analysis.

[36] J. Mork, Y. Chen, and M. Heuck, Photonic Crystal Fano Laser: Terahertz Modulation and Ultrashort Pulse Generation, Phys. Rev. Lett. **113**, 163901 (2014).

[37] Y. Yu, W. Xue, E. Semenova, K. Yvind, and J. Mork, Demonstration of a self-pulsing photonic crystal fano laser, Nat. Photon. **11**, 81 (2017).

[38] M. Günay, Z. Artvin, A. Bek, and M. E. Tasgin, Controlling steady-state second harmonic signal via linear and nonlinear Fano resonances, J. Mod. Opt. **67**, 26 (2020).

[39] M. Février, P. Gogol, A. Aassime, R. Mégy, C. Delacour, A. Chelnokov, A. Apuzzo, S. Blaize, J.-M. Lourtioz, and B. Dagens, Giant coupling effect between metal nanoparticle chain and optical waveguide, Nano Lett. **12**, 1032 (2012).

[40] H. Wang, Y. Wang, Y. Wang, W. Xu, and S. Xu, Modulation of hot regions in waveguide-based evanescent-field-coupled localized surface plasmons for plasmon-enhanced spectroscopy, Photon. Res. **5**, 527 (2017).

[41] I. Abdulhalim, Coupling configurations between extended surface electromagnetic waves and localized surface plasmons for ultrahigh field enhancement, Nanophotonics **7**, 1891 (2018).

[42] A. R. Rashed, B. C. Yildiz, S. R. Ayyagari, and H. Caglayan, Hot electron dynamics in ultrafast multilayer epsilon-near-zero metamaterials, Phys. Rev. B **101**, 165301 (2020).

[43] S. Schwarz, A. Kozikov, F. Withers, J. K. Maguire, A. P. Foster, S. Dufferwiel, L. Hague, M. N. Makhonin, L. R. Wilson, A. K.

Geim *et al.*, Electrically pumped single-defect light emitters in WSe_2, 2D Mater. **3**, 025038 (2016).

[44] J. Müller, J. M. Lupton, P. G. Lagoudakis, F. Schindler, R. Koeppe, A. L. Rogach, J. Feldmann, D. V. Talapin, and H. Weller, Wave function engineering in elongated semiconductor nanocrystals with heterogeneous carrier confinement, Nano Lett. **5**, 2044 (2005).

[45] I. I. Vlasov, A. A. Shiryaev, T. Rendler, S. Steinert, S.-Y. Lee, D. Antonov, M. Vörös, F. Jelezko, A. V. Fisenko, L. F. Semjonova *et al.*, Molecular-sized fluorescent nanodiamonds, Nat. Nanotechnol. **9**, 54 (2014).

[46] M. Premaratne and M. I. Stockman, Theory and technology of SPASERs, Adv. Opt. Photon. **9**, 79 (2017).